Atmospheric effects on the adhesion and friction between non-hydrogenated diamond-like carbon (DLC) coating and aluminum – A first principles investigation

ARTICLE *in* SURFACE SCIENCE · AUGUST 2006

Impact Factor: 1.93 · DOI: 10.1016/j.susc.2006.05.008

3 AUTHORS, INCLUDING:

Yue Qi
Michigan State University
110 PUBLICATIONS **2,480** CITATIONS
SEE PROFILE

Erkan Konca
Atilim University
15 PUBLICATIONS **369** CITATIONS
SEE PROFILE

Available online at www.sciencedirect.com
SCIENCE DIRECT
Surface Science 600 (2006) 2955–2965
SURFACE SCIENCE
www.elsevier.com/locate/susc

Atmospheric effects on the adhesion and friction between non-hydrogenated diamond-like carbon (DLC) coating and aluminum – A first principles investigation

Yue Qi [a,*], Erkan Konca [b], Ahmet T. Alpas [b]

[a] *Materials and Processes Lab, GM R&D Center, MC 480-106-224, Mound Road, Warren, MI 48090-9055, United States*
[b] *NSERC/General Motors of Canada Industrial Research Chair, University of Windsor, Windsor, ON., Canada N9B 3P4*

Received 14 December 2005; accepted for publication 2 May 2006
Available online 2 June 2006

Abstract

Experimentally, non-hydrogenated DLC coatings were tested against 319 Al alloy in the nitrogen, hydrogen, dry air (0% RH), and ambient air (40% RH) environments using a vacuum pin-on-disc tribometer. The average coefficient of friction (COF) and the material transfer changed dramatically depending on the test environment. Density functional theory (DFT) calculations were performed to investigate the interaction of diamond surface, to represent non-hydrogenated DLC, with N_2, H_2, and H_2O molecules. These calculations suggested that hydrogen and water would dissociate and be chemically adsorbed at a diamond surface whereas the dissociation of nitrogen is very unlikely to happen. Therefore, the diamond/DLC surface is passivated by –H termination in hydrogen and by –OH termination in water vapor, but not passivated in nitrogen. The calculated work of separation for Al with non-passivated and reacted diamond surfaces indicated the same tendency of adhesive transfer as observed in the pin-on-disc tests. The calculated work of separation at the interfaces formed after material transfer has the same trend with the measured COF. Therefore, DFT calculations successfully explained the atmospheric dependency of the tribological behavior of non-hydrogenated DLC coatings.

Keywords: Density functional calculations; Aluminum; Diamond-like carbon; Adsorption; Adhesion; Friction

1. Introduction

The excellent tribological properties of crystalline diamond and amorphous diamond-like carbon (DLC) have stimulated substantial interest in their application as low temperature, wear-resistant coatings for tools and machine elements [1–4]. Lower surface roughness, lower deposition temperatures and fewer problems with their adhesion to the substrates are among the main advantages of DLC coatings over diamond. In addition to their low coefficient of friction (COF) and low wear rate, the anti-sticking property of DLC coatings to aluminum has generated interest in using them as tool coatings for dry machining of aluminum alloys [5,6].

DLC is a mixture of sp^2 and sp^3 hybridized bonds with varying amounts of adsorbed (i.e. chemically bonded and/or mixed) hydrogen. A great deal of research has been carried out towards understanding the origin of the diverse tribological behavior of the various kinds of DLC coatings in terms of the adhesion, friction and wear properties. It has been shown that the tribological behavior of these coatings depends on the bond structure, namely the ratio of sp^2 to sp^3 bonding [7], hydrogen content [8–14], dopant content [15,16], loading conditions, humidity, and the test atmosphere [17–23]. Among various test atmospheres, hydrogen and water play important roles in changing the tribological behavior of DLC coatings with or without hydrogen [24]. Extensive tribological tests on DLC coatings in various atmospheres (ambient air, dry air, vacuum) showed that

* Corresponding author. Tel.: +1 586 947 0751; fax: +1 586 986 8697.
E-mail address: yue.qi@gm.com (Y. Qi).

0039-6028/$ - see front matter © 2006 Elsevier B.V. All rights reserved.
doi:10.1016/j.susc.2006.05.008

the presence of a sufficient amount of hydrogen in the DLC film structure is the most critical intrinsic factor determining the tribological behavior of the DLC coatings [9,12,14]. In vacuum, for example, the DLC films containing sufficient amounts of hydrogen give very low COF values (0.01 and lower) and low wear rates (1×10^{-8} mm^3/m and lower); on the other hand, non-hydrogenated DLC coatings experience high COF values (>0.5) and high wear rates under the same conditions. The origin of the high COF of the non-hydrogenated DLC films in vacuum was attributed to the interaction of the ''dangling bonds'' of carbon atoms with the counter surface [9,12]. For hydrogenated DLC films, it has been generally agreed that this interaction is eliminated by hydrogen atoms that bond with the carbon atoms on the surface thereby passivating the otherwise reactive surface [9,13,25]. In the presence of water vapor, DLC films without hydrogen in their structure showed low COF and low wear rates [22,25]. On the other hand, introduction of water vapor into the test chamber increased both COF and wear rate of the hydrogenated DLC films [26,27]. The changes in the friction, wear and adhesion behavior of DLC coatings at different test environments indicate that chemical and physical changes occur on the DLC surface and at the Al/DLC sliding interface.

First principles calculations provide details of electronic structures of the system, thus offer insights into the surface and interface chemistry, interface structures and adhesion properties. However, due to the complexities associated with modeling amorphous structures, there is a paucity of reported computational studies on the properties of DLCs. Of relevance to the present work are: Clark et al. [28], who compared structures for amorphous silicon and carbon and found five fold neighbors only in amorphous silicon but not in amorphous carbon; Marks et al., who demonstrated three- and seven-member ring structures in tetrahedral amorphous carbon (ta-C) using ab initio molecular dynamics [29]; Valladares et al., who modeled tetrahedral amorphous clusters up to 59 atoms doped with N atoms using density functional theory (DFT) [30]; Koivussaari et al., who found that even in sp^3 rich tetrahedral amorphous carbon (ta-C), the surface has a graphitic reconstruction [31]; Dag and Ciraci recently modeled the sliding friction between H-terminated diamond (0 0 1) surfaces, and reported the repulsive interaction due to H termination [32]. To the best of our knowledge, there has not been a publication on first principles study of the effect of test environment on adhesion and friction between DLC and aluminum.

Since DLC is a mixture of sp^2 and sp^3 hybridized bonds, it is reasonable to use graphite and diamond to represent regions with fully sp^2 or sp^3 bonds and interpret the properties of DLC from such calculations. In modeling of the adhesion between Al and diamond or graphite interfaces, Qi et al. found that Al tends to transfer to a clean diamond surface, but does not transfer to hydrogen passivated diamond surface [33]. On the other hand, graphite will transfer to the Al surface layer by layer [34]. These results are consistent with experimental observations that Al adheres to the non-hydrogenated DLC coating surface and causes its high friction and wear in inert environments [35]. These results also suggest a wear mechanism for DLC. Since DLC can graphitize during dry sliding [36], the newly formed graphite layer will transfer to the Al surface. However, as the interaction between Al and graphite is weak, the graphite layer can fall off from the Al surface (and contribute to wear track debris), and perhaps would be replaced with another graphite layer.

In modeling of surface reactions with diamond, Kern et al. have shown that H will change the diamond (1 1 1) 2×1 surface into 1×1 configuration [37]. Larsson and Lunell calculated the adsorption energies of halogen terminated diamond and found that the adsorption energies were much larger for the H and F species than for other species like Cl and Br [38]. They also calculated the adsorption energies of hydrocarbons on a diamond surface and found that their values were in the order of $C_2H > H > CH_2 > CH_3 > C_2H_2$ [39]. In modeling of surface reactions with graphite, Sha and Jackson have found that atomic hydrogen can be physically and chemically adsorbed at the graphite (0 0 0 1) surface using spin-polarized DFT [40]. Although these calculations were not intended to model DLC surface, one can infer from this work that it is very likely to have H atoms adsorbed at the DLC surface, since hydrogen can react with both diamond and graphite. However, there is very limited information on the adsorption states of N_2 and H_2O on either diamond or graphite surfaces.

Although the non-hydrogenated DLC structure has a complicated mixture of sp^2 and sp^3 bonded carbon atoms, the experimentally observed strong adhesion between DLC and aluminum (especially in vacuum) is thought to be due to the strong bonding formed between Al and the dangling bonds of carbon atoms of the DLC surface. In previous modeling, the strong covalent bonds at Al/diamond (1 1 1) interface indeed led to the adhesive transfer of Al to diamond surface. It is therefore reasonable to use the non-reconstructed diamond (1 1 1) surface as a model surface for the non-hydrogenated DLC surface, since the dangling bonds at a diamond surface have local bonding structure similar to those at a non-hydrogenated DLC surface. A similar approach was taken by Dag and Ciraci when they used H-terminated diamond (0 0 1) surface to model the interaction between H:DLC surfaces [32]. Another reason for choosing diamond (1 1 1) is that our previous calculations demonstrated that although diamond (1 1 1) will reconstruct into a (2×1) structure, upon exposure to Al, the diamond surface will de-reconstruct to form stronger interface bonds with Al. Therefore, the interface formed between Al/diamond is more likely to be Al/diamond (1 1 1)_1×1 instead of Al/diamond (1 1 1)_2×1 [33].

In this study, we investigated the friction and adhesion behavior of non-hydrogenated DLC coatings against 319 Al alloy in H_2, N_2, dry air and ambient air environments. The 319 Al is a typical cast aluminum–silicon alloy for

which the use of DLC as a tool coating in their machining is anticipated. It is expected that successful application of DLC coatings to drill bits will greatly minimize adhesion transfer, tool damage and process interruption, thereby eliminating the need for metalworking fluids. We have found that the COF was reduced in hydrogen and ambient air, but not in nitrogen. This indicates that reactions occurred at the sliding interface in these environments. To explain how different gas molecules change the tribological behavior at Al/non-hydrogenated DLC interface, we conducted DFT calculations. The modeling work was separated into two steps. First, we simulated the adsorption of the H_2, N_2 and H_2O at the diamond (1 1 1) surface (C surface) to understand whether or not chemical reaction will occur at the surface leading to surface passivation. Second, the work of separation at the interface between Al and the reacted C surfaces (Al/C interface), and the interface between the same reacted C surfaces (C/C interface) is computed. The purpose of this step is to illustrate how the adhesion and friction behavior will change at Al/non-hydrogenated DLC interfaces in different gas environments.

2. Experimental observations

2.1. Methods: materials and test conditions

DLC coatings (Teer Coatings Graphit-iC™) of 1.9 ± 0.1 μm thickness were received from Teer Coatings Ltd. (Worcestershire, UK). They were deposited on hardened (60 ± 2 Rockwell C) M2 high speed tool steel (in wt.%, 0.83% C, 4% Cr, 2% V, 6% W, 5% Mo, 0.27% Mn, 0.35% Si, and the balance Fe) discs from graphite and chromium targets using an unbalanced magnetron sputtering system (Teer UDP 650). The deposition, characterization, and some aspects of the tribological behavior of this particular type of DLC coating have been previously reported [41,42]. Raman spectrum of the as-deposited DLC did not have any sharp peaks [43]. Rather, it had an unresolved broad band between 1000 and 1800 cm^{-1}, which indicates that the film was amorphous with mainly sp^2 bonding. The mechanical properties of the DLC coatings were determined using the NanoXP nanoindenter with a Berkovich type indenter according to the Oliver and Pharr procedure [44]. The hardness and the elastic modulus values of the coating were measured as 16 and 147 GPa, respectively. Using the optical surface profilometer (Wyko NT 3300), the surface roughness (R_a) of the coatings was measured as 18 nm. The hydrogen content of the DLC coating was measured to be 1.28 at.% using the elastic recoil detection technique. Therefore, the DLC coatings can be described as Cr containing, sp^2 rich, non-hydrogenated DLC coatings.

A vacuum tribometer was used for the pin-on-disc tests. T5-heat treated 319 Al pins rounded to 4 mm diameter at one end were used as the counterface material sliding against the non-hydrogenated DLC coatings. A constant load of 5 N and a sliding speed of 0.12 m/s (125 rpm) were used in all tests. Tests were conducted in ambient and dry air (40% RH and 0% RH), nitrogen, and hydrogen–helium mixture (40 vol.% H_2–60 vol.% He) environments. For the tests under nitrogen, the chamber was evacuated to 3.99×10^{-3} Pa or lower before the gas was introduced. For the tests in 40% H_2–60% He, prior to the introduction of the gas, the chamber was evacuated to 3.99×10^{-3} Pa, vented with nitrogen, and evacuated to the same pressure level again to minimize any residual air and water vapor in the chamber. All tests were performed at 1 atm pressure. The pin-on-disc tests in 40% H_2–60% He will be referred to as hydrogen tests thereafter in the text.

2.2. Experimental results

Fig. 1 shows the COF curves of the non-hydrogenated DLC coatings in various gas environments. The lowest COF and wear of the non-hydrogenated DLC coatings against 319 Al were observed in the hydrogen environment. Initially, a high COF (0.70 ± 0.10) regime that lasted 50–250 revolutions was observed at the start of the tests in hydrogen (Fig. 1). Afterwards, the COF dropped to very low values around 0.015. Examination of the sliding track of the DLC coating tested in the hydrogen environment showed that the sliding track was smooth and there was a slight amount of wear which probably occurred during the initial high COF period. The examination of the contact surface of the 319 Al pin that was run against the non-hydrogenated DLC in hydrogen at 0.12 m/s showed the presence of a carbonaceous transfer layer (Fig. 2a and b). Therefore, when the COF was very low, the non-hydrogenated DLC was running against this transfer layer, not against the bare 319 Al pin surface.

The highest COF and wear rate of the non-hydrogenated DLC coatings were observed in the nitrogen environment. The average COF between the non-hydrogenated DLC coating and the 319 Al pin was 0.72 in nitrogen

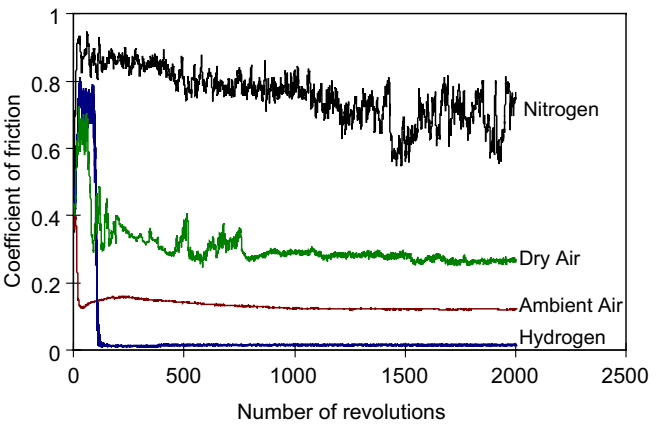

Fig. 1. The COF curves of the 319 Al/non-hydrogenated DLC sliding pair tested in N_2, H_2, dry air and ambient air (40% RH). The applied load and sliding speed were 5 N and 0.12 m/s.

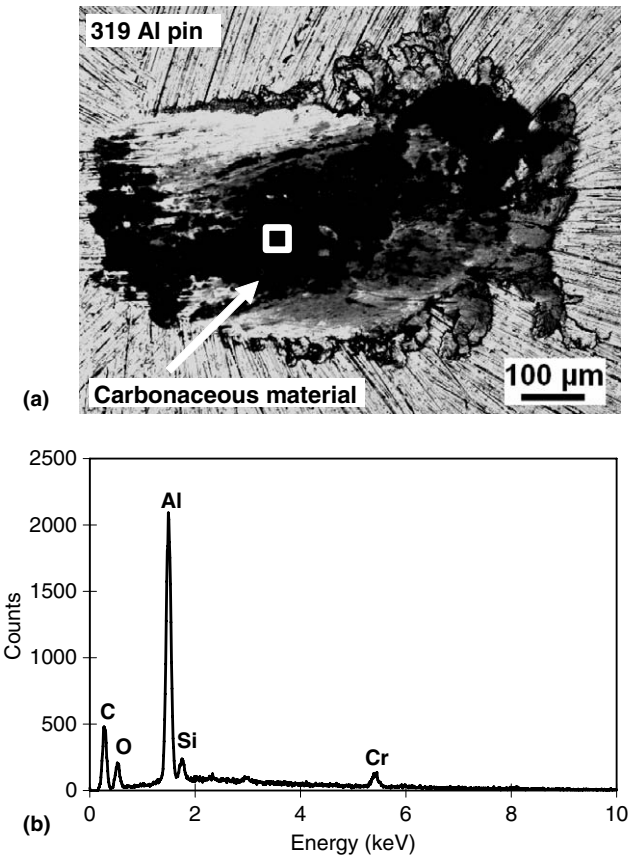

Fig. 2. (a) The backscattered electron SEM image of the contact surface of the 319 Al pin that was run against the non-hydrogenated DLC in 40% H_2–60% He environment, and (b) the EDS analysis of the location indicated in (a). The applied load and sliding speed were 5 N and 0.12 m/s.

(Fig. 1). Also, adhesive transfer of the 319 Al alloy to the non-hydrogenated DLC coating surface was observed as shown in Fig. 3. EDS analyses showed that the contact surface of the 319 Al pins tested against the DLC coating was a mixture of the 319 Al and the material removed from the DLC coating (C and Cr).

The non-hydrogenated DLC coatings showed intermediate COF values in dry air and ambient air. The steady state COF was 0.12 in ambient air (40% RH), which is lower than the average COF of 0.28 in dry air, as shown in Fig. 1. Some oxidized loose debris was formed, which accumulated along the edge of the wear track. There was no adhered Al on the wear track of the non-hydrogenated DLC coatings at the end of the tests in dry or ambient air. Similar to the tests in hydrogen, a distinct transfer layer formation was observed on the contact surface of the 319 Al pins tested in ambient air. The EDS analysis of this layer showed C, Cr and O peaks.

In summary, Fig. 1 shows that, dry air ($N_2 + O_2$), ambient air ($N_2 + O_2 + H_2O$), and H_2 reduced the COF and prevented material transfer to the non-hydrogenated DLC surface when run against 319 Al. The only exception was the N_2 atmosphere. It is suggested that O_2, H_2O and H_2 were chemically adsorbed on the non-hydrogenated

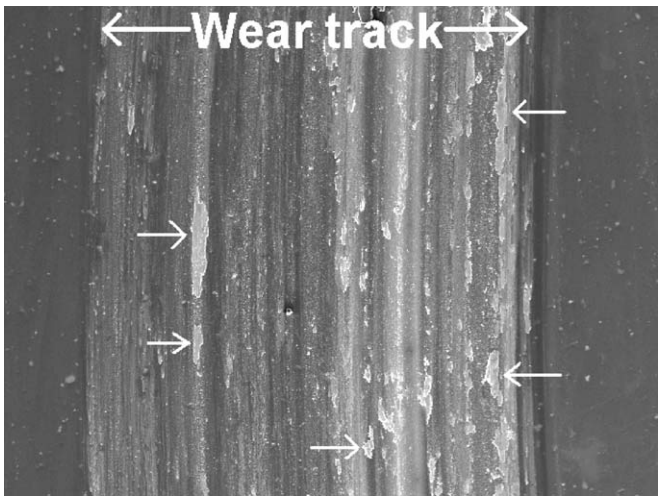

Fig. 3. The SEM image of a region of the wear track of the non-hydrogenated DLC coating tested against 319 Al alloy in nitrogen for 3.5×10^4 revolutions. Transfer of aluminum to the DLC coating surface, as indicated by the arrows, was observed. The applied load and sliding speed were 5 N and 0.12 m/s.

DLC surface that caused the passivation of the dangling bonds of the surface carbon atoms of the non-hydrogenated DLC coating. This process, in turn, prevented any strong bond formation between Al and the non-hydrogenated DLC surface, therefore reduced the COF.

However, the idea that chemical adsorption occurs at the non-hydrogenated DLC surface needs to be clarified. For this purpose, first principles based calculations were performed to investigate the interaction of non-hydrogenated DLC surface with N_2, H_2, H_2O molecules. The study of the interaction of O_2 with the non-hydrogenated DLC surface is not included in this work because this interaction is more complex than the other gaseous species and that H_2O had greater influence on the COF than O_2.

3. First principles calculations

3.1. Simulation methods

The Vienna ab initio Simulation Package (VASP) [45,46] was used to calculate the ground state energy and geometry of each configuration. The generalized gradient approximation (GGA) of Perdew and Wang [47] was used for the exchange-correlation energy functional. Potentials constructed with the projector-augmented wave (PAW) method [48] were used for C, H, O and N. A norm-conserving pseudopotential [49,50] with a cutoff radius of 0.96 Å was used for Al since its cutoff energy is closest to that of the other elements in the cell. Energy convergence of 1–2 meV/atom was obtained with a plane wave cutoff energy of 450 eV. The electronic degrees of freedom were converged to 10^{-5} eV/cell, and the Hellman–Feynman forces were relaxed to less than 0.03 eV/Å via the conjugate gradient method [51].

As a check of the computational methodology, we have separately computed lattice constants, cohesive energies, and elastic constants of bulk Al and diamond. We also computed surface energies of Al (1 1 1) and diamond (1 1 1). For the gases, we checked their cohesive energy and bond lengths for an isolated molecule in a hexagonal unit cell. Close agreement between the theoretical calculations and reported experimental values was noted, with the difference ranging from 0.5% to 5%.

A slab model was used to represent the diamond surface. Previous studies demonstrated that a slab of five double-layers of diamond with 10 Å vacuum separation was sufficient to give converged surface energy. Considering that the gas coverage is low, we put one molecule in each (2×2) diamond surface cell, ($5.048\times5.048\times24$ hexagonal cell). This resulted in a coverage of 1/4 monolayer. The simulation cell was also large enough to prevent interactions between molecules in the image cells, since the single molecule convergence tests suggested that the simulation cell should be larger than 5 Å.

To build Al/diamond interface with minimal lattice mismatch, the interface geometry was chosen as $(1\,1\,1)[1\,1\,\bar{2}]_{Al}\|(1\,1\,1)[1\,0\,\bar{1}]_{C}$, which was constructed by matching a (2×2) diamond (1 1 1) surface unit cell on top of a Al (1 1 1) supercell containing 3 units, with Al $[1\,1\,\bar{2}]$ aligned with diamond $[1\,0\,\bar{1}]$. The length of a (2×2) diamond (1 1 1) is 5.0534 Å, and the length of the Al super cell is 4.946 Å, which leads to a mismatch less than 2%, so that misfit dislocations could be ignored. The in-plane cell dimensions of the as-cleaved Al (1 1 1) slabs were then slightly increased to match the surface area of the diamond slabs. The simulation cell of Al/C interface contained 10 layers of Al and 6 layers of bi-layer carbon without vacuum, with fully periodic boundary condition two interfaces were formed inside the simulation cell. The inversion symmetry of the structure ensured that the interface energy was uniquely defined. The C/C interface was between two carbon slabs, each containing 5 bi-layers of C (1 1 1) planes with termination atoms at the surface. The slabs were surrounded by 10 Å vacuum to preclude interface from free surfaces. Both cell structures (with/without vacuum) were used to calculate the work of separation and gave consistent results [33]. A gamma centered K-grid $(8\times8\times1)$ was used for all the hexagonal unit cells to give converged energy.

3.2. Gas molecule adsorption at diamond (1 1 1) surface

Various binding sites are available for a gas molecule on the diamond (1 1 1) surface. Those sites with higher symmetries normally will provide lower binding energy. Examples of such sites are: the top site, which directly on top of one carbon atom of the top layer (grey atoms in Fig. 4), the bridge site, where the molecule or atom is shared by the two nearest-neighbor carbon atoms at the top surface, and the hole site, which is directly on top of a carbon atom in the second layer (black atoms in Fig. 4). We have tested different configurations of the gas molecules relative to the diamond (1 1 1) surface, including the different binding sites and the angle between the molecule and the surface. Since the goal is to find out the possibility of these molecules to react with the surface, only the configurations with the lowest energy barrier (which suggest the highest possibility of reaction) were reported. The top views of the binding sites of the three molecules on the diamond surface are shown in Fig. 4. Note that H_2 and N_2 occupy the bridge site, where the molecule was in parallel to the surface; H_2O pointed its O atom to the top site while the two H atoms were in parallel to the surface. It should be pointed out that the two H atoms were not symmetric in their placement, one H was on top of a C–C bond, and the other H was bisecting the two C–C bonds, respectively. To distinguish the H atoms, they are labeled as H1 and H2, respectively in the following discussion.

Since the molecules were at different binding sites, we defined the distance from the molecule to the diamond surface according to their configurations. The distance (d) was defined as the distance normal to the *xy* plane, which is the plane in parallel to the diamond surface. For N_2 and H_2, it was the normal distance between the center of the molecule to the center of the two closest carbon atoms at the surface that were bridged by the molecule. For H_2O, it was the dif-

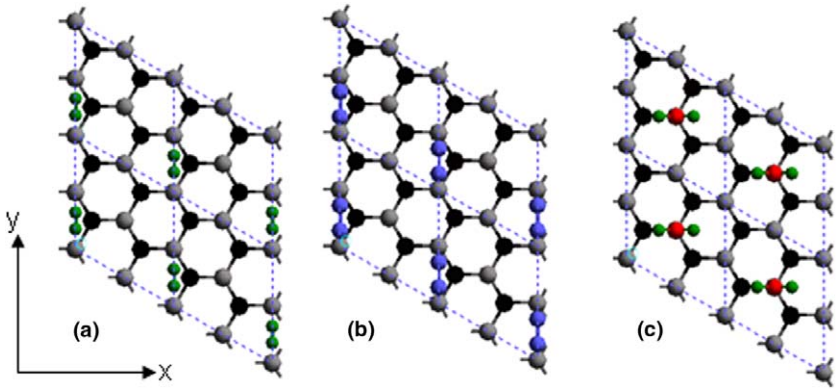

Fig. 4. Top views of the binding sites of (a) H_2, (b) N_2, and (c) H_2O on the diamond surface. The gray atoms are carbon atoms at the top surface, the black atoms are the atoms at the sub-top surface, green atoms are H, blue atoms are N, and red atom is O.

ference of z positions of the oxygen atom and the carbon atom under it.

All molecules were initially placed at 5 Å atop the diamond surface. Then, they were brought closer to the surface followed by structural minimization. During minimization, the distance of a molecule to the surface was kept constant. To achieve a constant distance, the z positions of the N_2/H_2 molecule and the two nearest carbon atoms were fixed for N_2/H_2. For the H_2O molecule, the z positions of the O atom and the carbon atom under it were fixed. However, these atoms were still allowed to move in the xy plane. During minimization, the atoms at the bottom of the slab were fixed in all three directions to ensure the slab mimicking the bulk effect of diamond. We first plotted the energy after each minimization as a function of the distance of the molecules to the surface. Although certain constraints were applied, the energy vs. distance curve gave guidelines for the reaction energy barriers from the minimized structures. The atomic configuration at the lowest energy position was then restarted and re-minimized allowing all the atoms in the system except the bottom layer to move freely. This led to the ground state with the lowest adsorption energy, which was referred as the "adsorption state" in the paper. Side views of the atomic structures at their adsorption state are shown in Fig. 5a–c, illustrating the distance between the molecule and the surface. The reference state was when the molecule was at 5 Å atop of the surface, which is also shown in Fig. 5 for comparison. The energy difference to the reference state was plotted as a function of the distance (d) between molecule and the diamond surface in Fig. 6. As the molecule approaching diamond (1 1 1) surface, the bond length (L) were changed due to the interaction with the diamond surface. Therefore, we also traced its value as a function of the distance to the surface.

In Fig. 6a, the initial bond length of H_2 molecule, (L(H–H)) at 5 Å away from the diamond surface is 0.751 Å, which is very close to the experimental bond length of H_2 in the gas phase (0.7466 Å [52]). This suggests no interaction of the molecule with the diamond surface or with the image molecules in the periodic cell. As the two H atoms approached the surface, the bond length of H_2 started to increase when the distance between the molecule and the surface became less than 3 Å, followed by a sub-

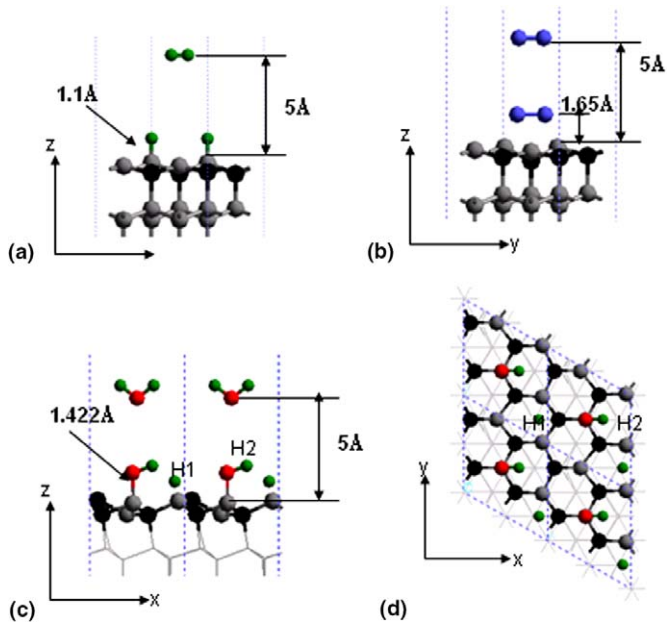

Fig. 5. Final configurations of H_2, N_2, and H_2O on the diamond surface.

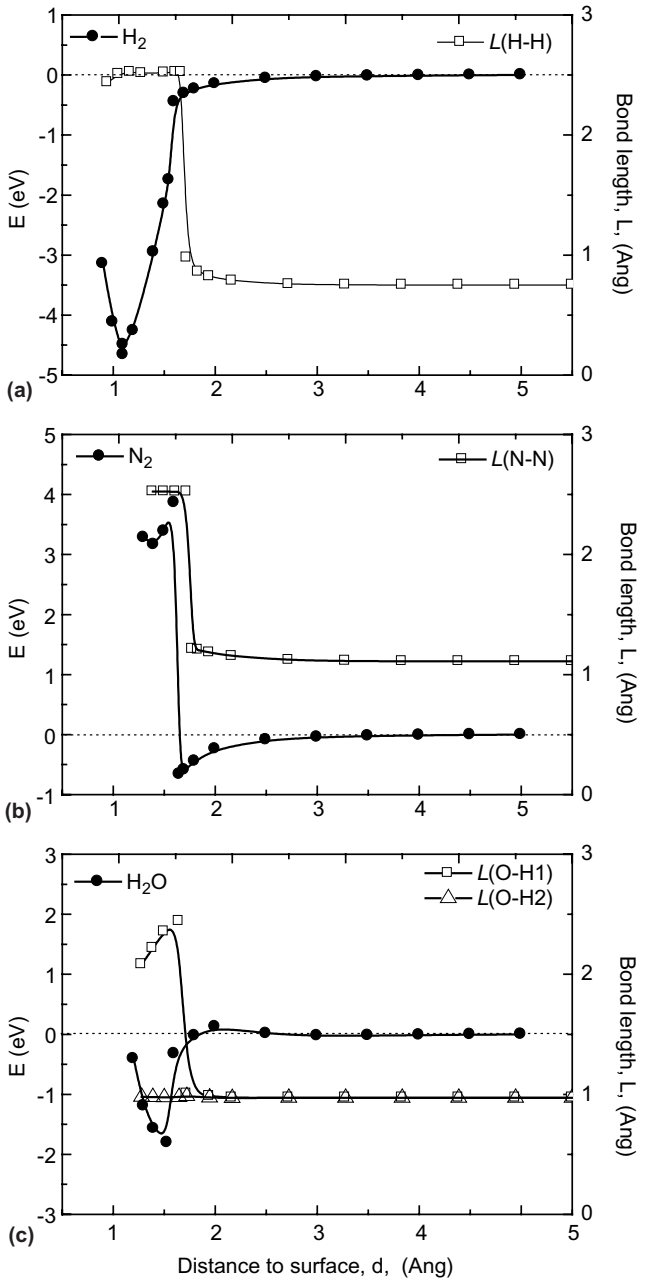

Fig. 6. The variation of the energy and bond length values of the H_2, N_2, and H_2O molecules as a function of their normal distance from the diamond surface.

stantial jump at $d = 1.55$ Å, indicating a fully dissociation of the H_2 molecule into two atomic H that bond with C atoms on the diamond surface. After dissociation, each H atom was directly on top of a carbon atom; therefore the distance between two H atoms is 2.524 Å, which is exactly the distance between the two nearest carbon atoms. When H_2 moves toward the surface, the energy is almost unchanged until it is less than 2.5 Å apart. Then, the energy started to decrease, especially when the distance is closer than 1.55 Å, after the H_2 is dissociated. The energy reaches a minimum around a distance of 1.1 Å, and at the fully minimized adsorption state the equilibrium bond distance of C–H is 1.099 Å. The energy is lowered by 4.50 eV compared to the non-adsorption state. During the dissociation process, there was no obvious energy barrier for this surface reaction. Thus, this reaction occurred spontaneously.

The initial bond length of N_2 at 5 Å away from the diamond surface was 1.110 Å (Fig. 6b). The experimental bond distance for N_2 in the gas phase is 1.0975 Å [52]. At the lowest adsorption state, the distance of N_2 to the diamond surface is 1.65 Å, but the distance between the two N atoms is still 1.213 Å. This is slightly increased from its molecular bond distance, but much smaller than the distance between the carbon atoms (2.524 Å). Therefore, N_2 stays as bonded. The adsorption energy is about 0.66 eV/molecule (63 kJ/mole). Typically, physical adsorption refers to an adsorption enthalpy on the order of 5–40 kJ/mol, and the enthalpy for chemical adsorption is 40–800 kJ/mol. For N_2, the calculated adsorption suggests a chemical adsorption with very low adsorption enthalpy. It is noticed that if the N_2 molecule was pushed closer to the surface, the minimized structure shows that N_2 could be dissociated, but the energy is 3.86 eV higher than the non-adsorption state. This implies that the dissociation of N_2 at the diamond surface is very unlikely to happen.

The reaction of the gas phase H_2O on the diamond surface is rather complicated since H_2O has two OH bonds. As previously noted, the two OH bonds have different configurations at the diamond surface. We plotted both the bond length for O–H1 and O–H2, as shown in Fig. 6c. When H_2O is 5 Å away from the diamond surface, both OH bonds have a length of 0.972 Å, compared well with the experimental value of 0.9584 Å [52]. As the water molecule approaches the surface, the O–H2 bond length does not change much but the O–H1 length increases to 2.4 Å, indicating that it is broken. The energy starts to increase when the water molecule is closer than 3 Å to the diamond surface. It then reaches a peak value of 0.122 eV around 2 Å, then the energy starts to drop until it reaches a minimum when the molecule is about 1.4 Å atop the surface. The adsorption energy is 1.8 eV/molecule (173 kJ/mol) and the C–OH bond length is 1.422 Å at the adsorption state. The minimized structure (in Fig. 5c and d) shows that water has dissociated into OH and H, while the OH is directed on top of a diamond at the surface and the H atom is at a bridge site for two carbon atoms, 1.504 Å apart from both carbon atoms. Therefore, H_2O is adsorbed and dissociated at the diamond (1 1 1) surface. The energy barrier is as small as 0.122 eV, suggesting this reaction is also likely to happen, but should be less favorable than the reaction of H_2 with diamond surface.

To further explore the bond character at the adsorption states, we employed the electron localization function (ELF), which is a position dependent function with a value that ranges from 0 to 1. ELF = 1 corresponds to localization (i.e. a covalent bond), and ELF = 0.5 corresponds to electron-gas like pair probability (i.e. a metallic bond). The ELF is undefined for values less than 0.5. The ELF contour plots of the reference state (5 Å away from the surface) and adsorbed states are compared in Fig. 7. Only the ELF contour plots along the planes that reveal the complicated bonding environment at the surface are shown. Hence, the ELF plots are shown in the *yz* plane for H_2 and N_2 in Fig. 7a and b, and in *xz* plane for H_2O in Fig. 7c. Specific ELF values are color-coded according to the figure legends, with ELF = 1 corresponding to red, ELF = 0.5 corresponding to a yellow–green, and ELF = 0 corresponding to blue, which are the regions of undefined ELF (e.g. the C atom cores or interstitial regions in the diamond slab). The atomic positions are also marked in each figure.

Fig. 7a shows that the strong covalent bond between the two H atoms is fully dissociated and redistributed into strong covalent bond between H and the surface C atom. N_2 has triple bonds in its gas phase: The ELF contour plot in Fig. 7b clearly shows the σ bond between the two N atoms, the lone pair inline with the two N atoms, and one π bond along the *yz* plane. When the N_2 molecule is adsorbed at the surface, it forms a complex C–N–N–C structure at the diamond surface, as shown in Fig. 7b. The lone pair is not in line with the molecule any more; rather, it is now being pushed away from the surface and form almost 45° angle with the molecule center line or the diamond surface. The covalent σ bond between the two N atoms remains undisturbed. There is a strong electron localization between the N atom and the C atom, which is due to the redistribution of the electrons in the N_2 π bonds and the dangling C bond at the surface. Therefore, the ELF plot suggests that N_2 is chemically adsorbed at the diamond surface, however the adsorption energy is very low and the N_2 is not dissociated. This suggests that the surface is not passivated during pin-on-disc test. In Fig. 7c, the H_2O molecule shows that the two strong covalent OH bonds and the lone pairs on the oxygen atom are pointing down to the diamond surface when the H_2O molecule is at the reference state. At the adsorption state, strong covalent bond forms between one C atom and the O, the OH bond forms an angle with the carbon surface, and the lone pair electrons on the oxygen shifts to the other side of the OH bond. However, the dissociated H atom is not chemically bonded to either of the

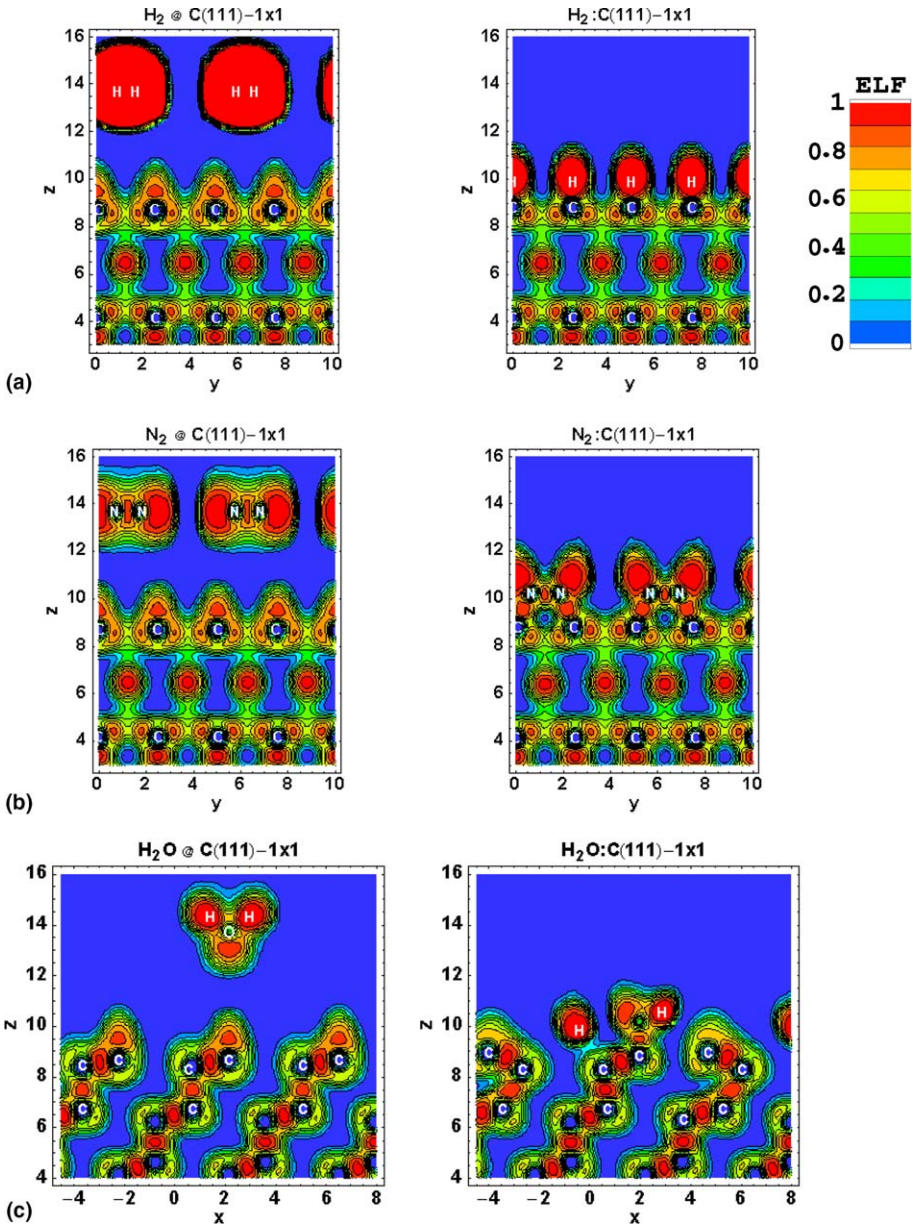

Fig. 7. Electron localization function contour plots for the un-adsorbed and adsorbed states of (a) H_2, (b) N_2, and (c) H_2O on the diamond surface.

carbon atoms, since there is no localized electron between them. Therefore, there are two possible surface termination configurations for H_2O at C(1 1 1) surface. In the first one, the H atom is thermally excited to a top site of a carbon atom and then chemically bonds with it, which can further lower the system energy to 3.79 eV compared to the non-adsorbed state. The distance between the OH group and the surface is unchanged by the adsorption of the H atom. The second configuration is a fully OH terminated diamond surface, since only the OH group is chemically bonded to the surface, the non-bonded H atom can combine with another non-bonded H atoms and leave the surface, leaving OH terminated C(1 1 1) surface. Depending on the chemical potential of water vapor, oxygen and hydrogen, the surface termination of diamond can be more complicated [53], as partially covered by –H and –OH. *Ab initio* calculations including these chemical potential terms may be used to develop a surface phase diagram for diamond in water [54]; however it is out of the scope of the current study. The monolayer –OH terminated diamond surface has been observed experimentally in chemical etching of diamond surface in oxygen and water vapor [55]. Since there will be oxygen and plenty of water vapor in air with 40% RH, we will assume that the diamond surface is fully OH terminated in the ambient air testing condition in the following calculations. We can expect the adhesion and friction behaviors of a partially –H and –OH terminated diamond surface to fall between fully –H and fully –OH terminated diamond surfaces.

3.3. Relationships between work of separation, adhesive transfer, and measured COF values

The first principles calculations have demonstrated that H_2 and H_2O will dissociate at the diamond surface but N_2 will not. After dissociation, the atomic H and OH will passivate the dangling bonds at the diamond surface, therefore preventing strong adhesion at the Al/diamond and Al/DLC interface. Although we did not calculate how the second molecule reacts with the surface and what the final coverage of the termination at the diamond surface is, as a model system we shall assume that the surface has reached 100% coverage to have a fully H terminated diamond surface in the H_2 environment, and fully OH terminated diamond surface in ambient air with water and oxygen, as suggested by experiments [55]. We also assume the non-passivated diamond surface for DLC in N_2 environment.

To simulate adhesion and adhesive transfer between these reacted surfaces with Al, we calculated the work of separation or ideal work of adhesion from DFT. Details of the work of separation (W_{sep}) calculation can be found in Ref. [33]. Work of separation characterizes the energy required to separate the interface into two free surfaces. The comparison of work of separation to the work of decohesion of the weaker material (Al in our case) would predict the likelihood of adhesive transfer. However, to predict the amount of adhesive transfer one has to apply a tensile test simulation to the interface structure. The calculated work of separation and the calculated adsorption energy are listed in Table 1 in comparison with experimental observations.

The calculated ideal W_{sep} at Al/non-passivated diamond interface is 4.5 J/m^2; at Al/H terminated diamond interface it is 0.02 J/m^2; and at Al/OH terminated diamond it is 0.2 J/m^2 for the interface. It has been shown that Al will transfer to a clean diamond surface but not to a H passivated diamond surface [32]. Here, for the OH terminated diamond surface, since the work of separation is an order of magnitude lower than the work of decohesion of Al (1.56 J/m^2), Al will not stick to OH terminated diamond (1 1 1) surface, nor to the DLC coating surface in the ambient air. This is in qualitative agreement with the experimental observation that there is a certain amount of Al transfer to the DLC surface in N_2 (Fig. 3), but none when the environment is either H_2O or H_2. It is interesting to notice that the W_{sep} is larger at the OH terminated interface than at the H terminated interface, which is also consistent with the experimental observation of a higher COF in ambient air with 40% RH than in H_2 environment (Fig. 1).

In nitrogen environment, although Al transferred to DLC surface, the pieces of Al debris did not cover the contact area. Therefore, we can assume that the final contact interface for the pin-on-disc test in N_2 gas is still between the Al and non-passivated diamond surface (Al/C(1 1 1)). We already calculated a high W_{sep} of 4.5 J/m^2 and a close interfacial separation of 1.8 Å. We observed that carbonaceous transfer layers formed on the 319 Al pin surface in H_2 (Fig. 2) and ambient air [56] after a running-in period. It is the carbonaceous transfer layer on the 319 Al pin the DLC coating runs against during the steady state sliding. For this reason, the interaction between the two reacted DLC surfaces is of interest. As a model system, we have calculated the W_{sep} at H-terminated-diamond/H-terminated-diamond and OH-terminated-diamond/OH-terminated-diamond interfaces to simulate the sliding in H_2 and ambient air, respectively. The equilibrium interfacial separation are above 3 Å for both H–C(1 1 1)/H–C(1 1 1) and OH–C(1 1 1)/OH–C(1 1 1) interfaces. The calculated W_{sep} is 0.008 J/m^2 for the H–C(1 1 1)/H–C(1 1 1) interface, and is 0.02 J/m^2 for the OH–C(1 1 1)/OH–C(1 1 1) interface. For both cases, the work of separation is relatively low compared to the other work of separation values calculated for various systems[34], therefore a low COF is expected. It is interesting to notice that the trend of higher work of separation corresponding to higher COF. The measured COF value in ambient air (0.12) was significantly lower than the one in nitrogen (0.72) but higher than the one in hydrogen (0.015). In summary, the DFT calculations offered first principles based explanations to the observed atmospheric dependency of the tribological behavior of the non-hydrogenated DLC coatings

Erdemir has proposed that it is possible to have a repulsive force between the H-terminated DLC sliding surfaces

Table 1
Comparison of experimental and modeling data for the Al/non-hydrogenated DLC coating pair tested in H_2, N_2 and air with 40% RH

System	Al/DLC in H_2	Al/DLC in N_2	Al/DLC in air (40% RH)
Adhesive transfer	DLC transfer to Al	Al transfer to DLC	DLC transfer to Al
Coefficient of friction	0.015	0.72	0.12
Adsorption energy (eV/molecule)	4.66	0.66	1.80
Dissociation status	Atomic H	No dissociation	Atomic OH
Reacted DLC surface	H terminated carbon surface	Carbon surface with dangling bonds	OH terminated carbon surface
Initial contact interface	Al/H–C(1 1 1)	Al/C(1 1 1)	Al/OH–C(1 1 1)
W_{sep} (J/m^2)	0.02	4.5	0.2
Interfacial separation (Å)	3.21	1.86	3.25
Final interface	H–C(1 1 1)/H–C(1 1 1)	Al/C(1 1 1)	OH–C(1 1 1)/OH–C(1 1 1)
W_{sep} (J/m^2)	0.008	4.5	0.02
Interfacial separation (Å)	3.02	1.86	3.12

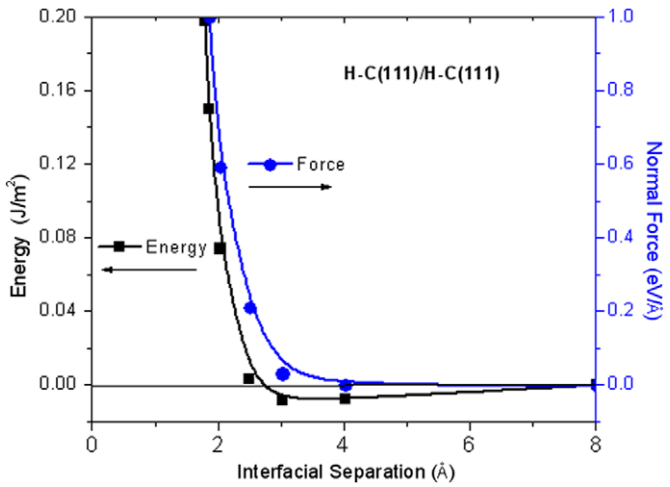

Fig. 8. Energy change and normal force at H–C(1 1 1)/H–C(1 1 1) interface.

[6]. Dag and Ciraci have shown a repulsive force between H terminated diamond (0 0 1) surfaces exists when the interface distance is smaller than 2.5 Å. As we simulated two H–C(1 1 1)/H–C(1 1 1) surfaces approaching each other, we calculated the system energy change as a function of the interfacial distance in Fig. 8. The reference state is the separated state of the two surfaces. The equilibrium interfacial separation is about 3 Å and energy released by the interface formation is 0.008 J/m^2 (also defined as the work of separation). The energy change becomes positive for the interfacial separation less than 2.5 Å. This positive energy change comparing to the separated state suggests the two free surfaces are energetically favored in the separated state. The normal force was then calculated from the numerical derivation of energy with respect to the interfacial separation. The attractive force is very small during adhesion process; on the other hand the repulsive force increases dramatically when the interface separation is closer than 2.5 Å. This repulsive force avoids the H-terminated carbon surfaces getting closer and consequently avoids any chemical bonding breaking and formation at the interface. Therefore, it leads to a very low COF, as measured in the pin-on-disc tests in hydrogen.

4. Conclusions

Non-hydrogenated DLC coatings were tested against 319 Al alloy in the nitrogen, hydrogen, dry air (0% RH), and ambient air (40% RH) environments using a vacuum pin-on-disc tribometer. The average COF was 0.72 in nitrogen, 0.28 in dry air, 0.12 in ambient air, and 0.015 in hydrogen. In an attempt to explain the varying friction and wear behavior of non-hydrogenated DLC coatings in these environments, DFT theory calculations were performed to study the interactions of nitrogen, hydrogen and water molecules with the diamond surface as a representative of the non-hydrogenated DLC coating. It is found that:

(1) The adsorption and dissociation of H_2 at the diamond surface is highly favored.
(2) For N_2, its dissociation at the diamond surface was found to be very unlikely to happen.
(3) H_2O dissociates at the diamond surface into OH and H where the OH is chemically bonded to the diamond surface and the H atom is at a bridge site between two carbon atoms.
(4) Electron localization function (ELF) calculations showed strong covalent bonding with diamond for H_2 and H_2O but not for N_2.
(5) The calculated ideal work of separation was 0.02 J/m^2 for the Al/H terminated diamond interface, 0.20 J/m^2 for the Al/OH terminated diamond (1 1 1) interface, and 4.5 J/m^2 for the Al/non-passivated diamond interface. These values indicated that Al would transfer to the clean diamond surface but not to the H or OH passivated diamond surfaces, as observed in the pin-on-disc experiments.
(6) A minimum work of separation (0.008 J/m^2) was calculated for the interface between H-terminated carbon surfaces. A repulsive force was found to increase dramatically as two surfaces were closer than 2.5 Å, thus leading to a very low COF, as measured during the tests in hydrogen environment.
(7) The work of separation at OH–C(1 1 1)/OH–C(1 1 1) interface is calculated as relatively low (0.02 J/m^2) compared to the other works of separation of other interfaces. Therefore a low COF is expected, but should be higher than H–C(1 1 1)/H–C(1 1 1). The measured COF value in ambient air (0.12) was significantly lower than the one in nitrogen (0.72) but higher than the one in hydrogen (0.015).

In summary, DFT calculations were successful in explaining the atmospheric dependency of the tribological behavior of non-hydrogenated DLC coatings against Al.

Acknowledgements

The authors wish to acknowledge the support of the General Motors High Performance Computing Team. The authors thank Dr. Lou Hector and Dr. Y-T Cheng for their invaluable discussions through out this work and attentive reading of the manuscript.

References

[1] J.D. Kim, Y.H. Kang, Int. J. Mach. Tools Manufact. 37 (8) (1997) 1155.
[2] R. Gahlin, M. Larsson, P. Hedenqvist, Wear 249 (2001) 302.
[3] R. Hauert, Tribol. Int. 37 (11-12) (2004) 991.
[4] S.V. Johnston, S.V. Hainsworth, Surf. Eng. 21 (1) (2005) 67.
[5] H.L. Coldwell, R.C. Dewes, D.K. Aspinwall, N.M. Renevier, D.G. Teer, Surf. Coat. Technol. 177–178 (2004) 716.
[6] H. Fukui, J. Okida, N. Omori, H. Moriguchi, K. Tsuda, Surf. Coat. Technol. 187 (1) (2004) 70.
[7] J. Robertson, Mater. Sci. Eng. R 37 (2002) 129.

[8] A. Grill, Wear 168 (1993) 143.
[9] C. Donnet, J. Fontaine, A. Grill, T. Le Mogne, Tribol. Lett. 9 (3–4) (2000) 137.
[10] H. Zaidi, J. Frene, A. Senouci, M. Schmitt, D. Paulmier, Surf. Coat. Technol. 123 (2000) 185.
[11] A. Erdemir, O.L. Eryilmaz, I.B. Nilufer, G.R. Fenske, Surf. Coat. Technol. 133–134 (2000) 448.
[12] A. Erdemir, Surf. Coat. Technol. 146–147 (2001) 292.
[13] A. Erdemir, Tribol. Int. 37 (2004) 577.
[14] H. Ronkainen, S. Varjus, J. Koskinen, K. Holmberg, Wear 249 (2001) 260.
[15] C. Donnet, Surf. Coat. Technol. 100–101 (1998) 180.
[16] Y.L. Su, W.H. Kao, J. Mater. Eng. Perform. 9 (1) (2000) 38.
[17] M.P. Delplancke-Ogletree, O.R. Monterio, Surf. Coat. Technol. 108–109 (1998) 484.
[18] J.A. Heimberg, K.J. Wahl, I.L. Singer, A. Erdemir, Appl. Phys. Lett. 78 (17) (2001) 2449.
[19] Y. Liu, A. Erdemir, E.I. Meletis, Surf. Coat. Technol. 86–87 (1996) 564.
[20] E. Yoon, H. Kong, K. Lee, Wear 217 (1998) 262.
[21] W. Zhang, A. Tanaka, K. Wazumi, Y. Koga, Thin Solid Films 413 (2002) 104.
[22] J. Andersson, R.A. Erck, A. Erdemir, Surf. Coat. Technol. 163–164 (2003) 535.
[23] J. Andersson, R.A. Erck, A. Erdemir, Wear 254 (2003) 1070.
[24] J. Fontaine, M. Belin, T.L. Mogne, A. Grill, Tribol. Int. 37 (2004) 869.
[25] B. Racine, M. Benlahsen, K. Zellama, M. Zarrabian, J.P. Villain, G. Turban, A. Grosman, Appl. Phys. Lett 75 (22) (1999) 3479.
[26] J. Jiang, S. Zhang, R.D. Arnell, Surf. Coat. Technol. 167 (2003) 221.
[27] C. Donnet, T. Le Mogne, L. Ponsonnet, M. Belin, A. Grill, V. Paetl, C. Jahnes, Tribol. Lett. 4 (1998) 259.
[28] S.J. Clark, J. Crain, G.J. Ackland, Phys. Rev. B 55 (1997) 14059.
[29] N.A. Marks, D.R. Mckenzie, B.A. Pailthorpe, M. Bernasconi, M. Parrinello, Phys. Rev. Lett. 76 (1996) 768.
[30] A.A. Valladares, A. Valladares, R.M. Valladares, M.A. McNeils, J. Non-Cryst. Solids 231 (1998) 209.
[31] K.J. Koivusaar, T.T. Rantala, J. Levosha, S. Leppavuori, Appl. Phys. Lett. 76 (2000) 2794.
[32] S. Dag, S. Ciraci, Phys. Rev. B 70 (2004) 241401.
[33] Y. Qi, L.G. Hector Jr., Phys. Rev. B 69 (2004) 235401.
[34] Y. Qi, L.G. Hector Jr., N. Ooi, J.B. Adams, Surf. Sci. 581 (2005) 155.
[35] E. Konca, Y.-T. Cheng, A.M. Weiner, J.M. Dasch, A.T. Alpas, Surf. Coat. Technol. 200 (5–6) (2005) 1783.
[36] Y. Liu, E.I. Meletis, J. Mater. Sci. 32 (1997) 3491.
[37] G. Kern, J. Hafner, G. Kresse, Surf. Sci. 366 (1996) 445.
[38] K. Larsson, S. Lunell, J. Phys. Chem. A 101 (1997) 76.
[39] K. Larsson, Phys. Rev. B 56 (1997) 15452.
[40] X. Sha, B. Jackson, Surf. Sci. 496 (2002) 318.
[41] S. Yang, D. Camino, A.H.S. Jones, D.G. Teer, Surf. Coat. Technol. 124 (2000) 110.
[42] S.K. Field, M. Jarratt, D.G. Teer, Tribol. Int. 37 (2004) 949.
[43] D. Camino, A.H.S. Jones, D. Mercs, D.G. Teer, Vacuum 52 (1999) 125.
[44] W.C. Oliver, G.M. Pharr, J. Mater. Res. 7 (6) (1992) 1564.
[45] G. Kresse, J. Hafner, Phys. Rev. B 49 (1994) 14251.
[46] G. Kresse, J. Furthmüller, Comput. Mater. Sci. 6 (1996) 15.
[47] J.P. Perdew, Y. Wang, Phys. Rev. B 46 (1992) 6671.
[48] P.E. Blöchl, Phys. Rev. B 50 (1994) 17953.
[49] A.M. Rappe et al., Phys. Rev. B 41 (1990) 1227.
[50] L. Kleinman, D.M. Bylander, Phys. Rev. Lett. 48 (1987) 1425.
[51] W.H. Press, S.A. Teukolsky, W.T. Vetterling, B.P. Flannery, Numerical Recipes in Fortran 90: The Art of Parallel Scientific Computing, second ed., Cambridge University Press, Cambridge, England, 1996.
[52] Handbook of Chemistry and Physics, 71st ed., CRC Press, 1991, p. 9-2.
[53] A. Laikhtman, A. Lafosse, Y. Le Coat, R. Azria, A. Hoffman, Surf. Sci. 551 (2004) 99.
[54] W. Zhang, J.R. Smith, X.-G. Wang, Phys. Rev. B 70 (2004) 024103.
[55] F.K. de Theije, M.F. Reedijk, J. Arsic, W.J.P. van Enckevort, E. Vlieg, Phys. Rev. B. 64 (2001) 085403.
[56] E. Konca, Y.T. Cheng, A. Weiner, J.M. Dasch, A.T. Alpas, Wear 259 (2005) 795.